



He, Ne and Ar systematics in single vesicles: Mantle isotopic ratios and origin of the air component in basaltic glasses

Aude Raquin*, Manuel Alexis Moreira, Fabien Guillon

Institut de Physique du Globe de Paris, Equipe de géochimie et cosmochimie, Université Paris Diderot et CNRS UM7154, 4 place Jussieu, 75005 Paris, France

ARTICLE INFO

Article history:

Received 5 February 2008

Received in revised form 7 July 2008

Accepted 9 July 2008

Available online 16 July 2008

Editor: R.W. Carlson

Keywords:

noble gases
mantle geochemistry
air contamination
laser ablation

ABSTRACT

An outstanding problem in understanding the origin of the gaseous phase, particularly the rare gas compositions in magmatic rocks, is the ubiquitous atmospheric component in bulk rock samples, and whether this atmospheric component is a late stage contamination of the sample, or a recycled component through sediments or altered oceanic crust. In the present study we address this problem by analyzing single vesicles from the “popping rock 2[D43” sample from the Mid-Atlantic Ridge using a UV laser ablation system. We have determined both elemental and isotopic compositions of He, Ne and Ar in single vesicles as well as Kr and Xe abundances. All vesicles analyzed have an isotopic composition identical to the referred degassed mantle value estimated from this same sample, despite analyzing vesicles from a wide size distribution. The atmospheric component, which is always detected in bulk samples by crushing or heating, was not detected in the single vesicles. This implies that the recycling of atmospheric noble gases in the mantle cannot explain the air-like component of this sample. The addition of the atmospheric component must occur either during the eruption, or after sample recovery.

© 2008 Elsevier B.V. All rights reserved.

1. Introduction

Understanding the distribution of helium, neon, argon, krypton and xenon in the mantle, both for elemental and isotopic compositions, is important for constraining the volatile acquisition and the evolution of Earth's surface reservoirs (Allègre et al., 1987; Allègre et al., 1983; Hiyagon et al., 1992; Kellogg and Wasserburg, 1990; Marty and Tolstikhin, 1998; Onions and Tolstikhin, 1996; Ozima and Zahnle, 1993; Porcelli and Wasserburg, 1995; Poreda and Farley, 1992; Sarda et al., 1985; Staudacher et al., 1989; Tieloff and Kunz, 2005). However, the interpretation of rare gas data has been challenging because of an air-like component in mantle-derived rocks. Rare gas data from a single sample generally displays a binary mixture between a mantle and an atmospheric component. The binary mixture is illustrated in Fig. 1, where neon isotope data from Mid Oceanic Ridge Basalt (MORB) and Oceanic Island Basalt (OIB) are plotted in the three-neon isotopes diagram (Allègre and Moreira, 2004). This mixture raises two important questions, which are still the subject of debate. The first is the origin of the air-like component. Several hypotheses have been postulated to elucidate this origin but there is still no general consensus. This component was first considered to be dissolved in the glassy matrix (Marty et al., 1983) as a result of interaction between seawater (where the atmospheric gases are dissolved) and magma before or during the eruption (Farley and Poreda, 1993; Fisher, 1997;

Patterson et al., 1990; Sarda et al., 1985). High precision crushing analyses of both MORB and OIB have revealed heterogeneity in rare gas isotopic compositions at a millimeter scale (Harrison et al., 1999; Moreira et al., 1998; Tieloff et al., 2003; Tieloff et al., 2002; Tieloff et al., 2000). The air-like component was therefore interpreted either as a late stage surface contamination during sampling or contamination during sample preparation in laboratories (Ballentine and Barfod, 2000) where modern air could be introduced into micro fractures and released during crushing (Mungall et al., 1996). Alternatively, this component has been interpreted as a component recycled in the mantle via subduction processes (Sarda, 2004) and mixed with the normal MORB source mantle. This concept of noble gas recycling has been suggested since the discovery of relationships between noble gases and trace elements in arc magmatism settings (Bach and Niedermann, 1998) and between noble gases and isotopic ratios (e.g. lead) in Mid-Atlantic Ridge basalts (Sarda et al., 1999). This hypothesis of noble gases recycling was reinforced by the work of Matsumoto and collaborators where data from paleo-arc settings seem to confirm a possible atmospheric noble gas recycling in the mantle wedge via the subduction process (Matsumoto et al., 2001). More recently, precise $^{124-126-128}\text{Xe}/^{130}\text{Xe}$ measurements in CO_2 well gases indicate a slight enrichment in the light isotopes of xenon, compared to the atmosphere suggesting an important recycling of atmospheric xenon in the mantle through geological times (Holland and Ballentine, 2006) and challenge the so-called “noble gases subduction barrier” which suggests that noble gases of the subducted oceanic crust (and sediments) are returned back to the atmosphere through arc volcanism (Staudacher

* Corresponding author.

E-mail address: raquin@ipgp.jussieu.fr (A. Raquin).

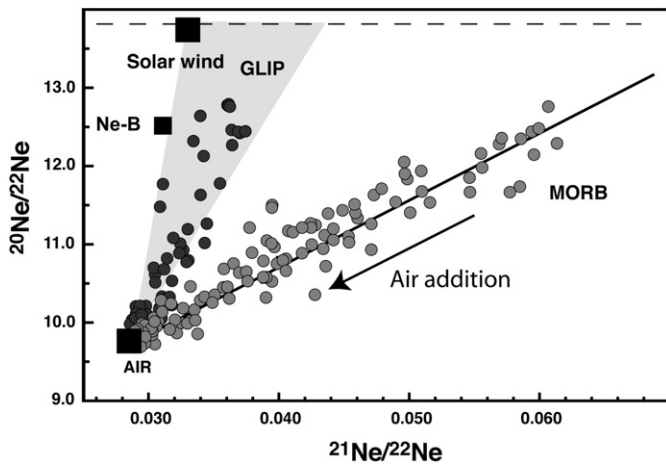


Fig. 1. The neon three isotopes diagram ($^{20}\text{Ne}/^{22}\text{Ne}$ versus $^{21}\text{Ne}/^{22}\text{Ne}$). Data are those used in Allègre and Moreira (2004) with the addition of unpublished data (Raquin and Moreira, 2005). The shaded region represents OIB data from Galapagos, Loihi, Island and Pitcairn (GLIP). MORB and OIB data plot on two different mixing lines between a mantle component and an ubiquitous atmospheric component. This air-like addition prevents knowing the exact $^{20}\text{Ne}/^{22}\text{Ne}$ value for the upper mantle: neon-B (12.5) or SW neon (13.8).

and Allègre, 1988). Hence, knowledge of the origin of this air addition is important to estimate the concentration of noble gases in the mantle and to calculate fluxes between Earth reservoirs. For example, if we consider data on sample 2][D43, as being the most representative for the upper mantle volatile content (Javoy and Pineau, 1991; Moreira et al., 1998; Pineau and Javoy, 1994; Staudacher et al., 1989) and, if air addition is only due to a superficial contamination, then the ^{36}Ar concentration in the mantle would be two orders of magnitude lower than if the air addition is due to recycling.

The second question that is raised by the three-neon isotopes diagram is the value of the stable and non-radiogenic $^{20}\text{Ne}/^{22}\text{Ne}$ ratio in the mantle. Although this was first considered to be similar to the solar wind neon (13.82 (Grimberg et al., 2006)) (Yokochi and Marty, 2004), such a high value is not recorded with confidence in mantle-derived rocks, because only a very small contamination from the air-like component is sufficient to cause large deviations from the solar neon isotope composition. A solar wind value implies a model where gases are trapped in the mantle during the Earth accretion by dissolution of solar wind gases in a magma ocean previously degassed (Harper and Jacobsen, 1996; Hayashi et al., 1979; Mizuno et al., 1980; Porcelli et al., 2001; Sasaki, 1999). However, this origin was challenged in recent studies and a component with a neon-B value (12.5 (Black, 1972)) has been proposed. Such a component is mainly recorded in gas rich meteorites and on the lunar regolith. This suggests that the Earth material precursors have acquired this signature by irradiation by the solar wind during an early stage of the solar nebula formation, such as during the T-Tauri phase (Ballentine et al., 2005; Raquin and Moreira, 2005; Tieloff et al., 2002; Tieloff et al., 2000).

Solving these two unknowns is important to improve models of the origin and evolution of volatile elements in the Earth. Knowing the real value of the $^{20}\text{Ne}/^{22}\text{Ne}$ ratio in the mantle will improve our understanding of how gases are trapped in the mantle and the quantification of the air addition will help to calculate correctly fluxes from mantle reservoirs.

The traditional analytical procedure such as total crushing or total fusion gives an average composition of gases trapped in basalt vesicles. An attractive alternative is to analyze single vesicles. This type of work was initiated by Burnard and collaborators, who gave the first noble gas results in single vesicles (Burnard, 1999b; Burnard et al., 1997). In the present study, a similar approach was used. Using a laser UV ablation system on the famous “popping rock” 2][D43 sample, we have determined both elemental and isotopic compositions of He, Ne and Ar in single vesicles as well as Kr and Xe abundances. The results

enable us to discuss the origin of the air-like rare gas component present in the MORB and OIB glasses.

2. Samples and analytical procedure

The sample 2][D43 called “popping rock” was dredged in the North Atlantic at $13^{\circ}46'\text{N}$ at a depth of 3500 m during the R/V “Akademik Boris Petrov” cruise in 1985. This sample has been the subject of many studies (Burnard, 1999a; Burnard et al., 1997; Javoy and Pineau, 1991; Moreira et al., 1998; Pineau and Javoy, 1994; Sarda and Graham, 1990; Staudacher et al., 1989). The main feature that makes this sample unique is the exceptionally high vesicularity (up to 18%) and the very high gas content. The vesicle size distribution has been well described in Sarda and Graham (1990) and Burnard (1999a) with small and large vesicles coexisting together (from 0.02 to 1.5 mm of diameter) implying that this sample has suffered minor coalescence or loss of any vesicles. Analysis of this sample by step crushing or step heating has revealed ^4He , ^{22}Ne , ^{36}Ar , ^{84}Kr and ^{130}Xe concentrations close, in that order, to 8×10^{-5} , 10^{-9} , 5×10^{-8} , 10^{-10} and 10^{-11} $\text{cm}^3\text{STP/g}$ (Moreira et al., 1998; Raquin and Moreira, 2005; Sarda et al., 1988; Sarda and Graham, 1990; Staudacher et al., 1989). For He, these concentrations are more than one order of magnitude more than typical MORB concentrations (Sarda and Graham, 1990).

The helium isotopic ratio is similar to the mean MORB value with a mean $^4\text{He}/^3\text{He}$ of 88,000 (or 8.2 Ra where Ra is the atmospheric $^3\text{He}/^4\text{He}$ ratio with a value of 1.384×10^{-6}) (Javoy and Pineau, 1991; Sarda et al., 1988; Staudacher et al., 1989). The $^{20}\text{Ne}/^{22}\text{Ne}$, $^{21}\text{Ne}/^{22}\text{Ne}$, $^{40}\text{Ar}/^{36}\text{Ar}$ and $^{129}\text{Xe}/^{130}\text{Xe}$ ratios vary between the atmospheric value and 12.5, 0.06, 28 000 and 7.5 respectively (Sarda et al., 1988; Staudacher et al., 1989; Kunz, 1999; Moreira et al., 1998; Raquin and Moreira, 2005). The $^4\text{He}/^{40}\text{Ar}$ is close to 1.5 and roughly similar to the theoretical production ratio using the mantle (U + Th)/K ratio (Allègre et al., 1987). In spite of the fact that this sample shows the trace element characteristics of E-MORB signature (Bougault et al., 1988), most studies agree that this sample is the most representative of the upper mantle volatile content and isotopic compositions.

This sample presents all the characteristics required for studying the origin of the air-like noble gas component trapped in basalts. As mentioned above, analyses by step crushing or step heating have revealed various isotopic signatures in the same piece of sample: the degassed mantle component, the air-like component and the mixture between these two latter. The air-like component is found preponderantly in the first step of analyses and the mantle component in the latest. The sites related to the air-like component must be easier to rupture during the extraction procedure than the site containing the mantle component (Ballentine and Barford, 2000; Sarda, 2004). It can be the largest pressurized vesicles.

The pioneer work of Burnard using a laser extraction technique in single vesicle has shown vesicles with a mantle component ($^{40}\text{Ar}/^{36}\text{Ar}$ as high as 40,000) but not the air-like component (Burnard et al., 1997). However, in their study, 300 μm thick sections have been made on the sample in order to visualize the vesicles to be open. This result is coherent with an air-like component located in the largest vesicles and lost during the thick section preparation.

Here, we processed large pieces of glass sample ($\sim 1 \text{ cm}^3$). This has the advantage of allowing analysis of all the range of vesicle sizes. In particular we were able to analyze the largest vesicles susceptible to contain the atmospheric component. The disadvantage, however is that vesicles are not visible before ablation.

After cleaning with ethanol and acetone, a piece of sample approximately one centimeter-size of fresh basalts was selected using a binocular. Samples are introduced in a vacuum cell connected through a valve to the purification line of the ARESIBO II mass spectrometer. The cell is then baked at 150°C over 48 h under ultra-high vacuum. A MKS baratron pressure system, which is sensitive at 10^{-4} Torr on a range of 10 Torr, is located in the volume of the cell allowing the measurement of the total gas pressure in a vesicle.

Gases are released by laser ablation using an ALTEX 300i (argon fluoride) UV laser, which has a wavelength of 193 nm. This wavelength is associated with a 4–6 ns pulse with a power of 2×10^6 W at a frequency of 100 Hz, permitting an ablation process without heat diffusion at the point of impact (Geertsen et al., 1994). Craters formed by the beam for a one-minute shot have a diameter of ~ 50 μm and depth of ~ 70 μm . Various ablation times are carried out in a random way on the sample. In many cases there is no vesicle under the surface of the sample and only a small volume of the matrix is ablated. Gases released from this latter volume have sometimes been purified and analyzed, but mostly when no vesicle was pierced the gases were pumped out of the cell, and another ablation was conducted. However, in the case when the ablation randomly pierces a vesicle, an immediate increase of the pressure is recorded in the cell. Gases are afterwards purified with one hot Ti getter (800 °C) and one cold SAES getter. Noble gases are trapped on charcoal at a temperature of ≈ 10 K. Finally, He, Ne, Ar ^{84}Kr ^{129}Xe and ^{130}Xe isotopes were analyzed on the ARESIBO II mass spectrometer. Kr and Xe are released with argon from the charcoal at 320 K. Masses 84, 129 and 130 are measured just after introduction in the mass spectrometer and before analyzing argon. ^4He and ^{40}Ar were collected on a Faraday cup, whereas ^3He , $^{20-21-22}\text{Ne}$, $^{36-38}\text{Ar}$, ^{84}Kr and $^{129-130}\text{Xe}$ isotopes were collected using an electron multiplier in ion counting mode. Correction of $^{40}\text{Ar}^{++}$ and CO_2^{++} were applied on mass 20 and 22 using the following ratios $^{40}\text{Ar}^{++}/^{40}\text{Ar}^+ = 0.085$ and $^{44}\text{CO}_2^{++}/^{44}\text{CO}_2^+ = 0.009$.

Blanks are of major importance because the quantity of rare gases contained in a single bubble can be very small. The ARESIBO II mass spectrometer and the purification line are made of Kovar glass, and during the experiment, helium diffuses through the walls. The ^4He blank amount is consequently directly proportional to the time of the experimental procedure of extraction and purification. These times must therefore be as short as possible. In addition, some gases are adsorbed on the surface of the sample. At the beginning of the study, shootings could last up to 6 min and the sample was not isolated from the purification line during experimentation. In these conditions, typical

blank values were respectively 8×10^{-9} , 5×10^{-12} and 2×10^{-11} cm^3STP for ^4He , ^{22}Ne and ^{36}Ar . Later, shootings have been limited to 1 min and a valve has been placed between the cell and the purification line to limit the contribution of gases adsorbed to the surface of the sample and diffusion of neon through the fused silica window. Blanks decreased to 4×10^{-9} , 5×10^{-13} and 8×10^{-13} cm^3STP for the same isotopes, an order of magnitude lower than without closing the valve.

Few blanks were performed just after introduction of the sample into the cell until the ^{22}Ne concentration stabilizes at 5×10^{-13} cm^3 . After a vesicle was decrepitated, we performed a new blank. Blank corrections have been done using the mean value, before and after the vesicle decrepitated.

Argon isotopic ratios have to be corrected because of the pressure effect on the mass discrimination. As an example, the argon amount released by a single vesicle is much smaller than the air standards. In order to address this issue, the mass discrimination was calibrated for a large range of ^{36}Ar content by inletting a variable number of air pipettes and by using different volumes of the line. For example on the $^{38}\text{Ar}/^{36}\text{Ar}$ ratio, for ^{36}Ar abundances higher than 2×10^{-11} cm^3 , mass discrimination is constant: 0.997 normalized to the atmosphere. For ^{36}Ar abundances lower than 2×10^{-11} cm^3 , a correction using a linear interpolation was applied on the mass discrimination because the latter is much higher: 1.020 (normalized to the atmosphere) for an introduced ^{36}Ar concentration of 2×10^{-12} cm^3 .

3. Results

CO_2 , He, Ne, Ar, Kr and Xe elemental abundances and He, Ne and Ar isotopic composition for each vesicle are given in Tables 1 and 2. ^4He abundances in single vesicle vary between 4×10^{-9} cm^3 (V13) and 4.7×10^{-7} cm^3 (V5) and are very well correlated to the pressure of gas released from the vesicle and recorded in the cell. The helium isotopic composition is very homogeneous for all vesicles (Fig. 2). The mean $^4\text{He}/^3\text{He}$ is $93,000 \pm 10,000$ (or 7.75 ± 0.86 Ra where Ra is the

Table 1
He, Ne, Ar, Kr and Xe abundances from laser extraction of single vesicles of the “Popping rock” 2[D43

| | Pcell (mTorr) | Laser time (min) | CO_2 ($\text{cm}^3 \times 10^{-5}$) | ^4He ($\text{cm}^3 \times 10^{-9}$) | ^{22}Ne ($\text{cm}^3 \times 10^{-13}$) | ^{36}Ar ($\text{cm}^3 \times 10^{-13}$) | ^{84}Kr ($\text{cm}^3 \times 10^{-14}$) | ^{129}Xe ($\text{cm}^3 \times 10^{-15}$) | ^{130}Xe ($\text{cm}^3 \times 10^{-15}$) |
|----------------------|------------------|---------------------|---|---|---|---|---|--|--|
| 2[D43 vesicle | | | | | | | | | |
| V1 | 50 | 1.5 | 106 | 35 | 6.3 | 43.4 | NA | NA | NA |
| V2 | 178 | 3.0 | 371 | 124 | 3.4 | 37.8 | NA | NA | NA |
| V3 | 482 | 2.5 | 1216 | 406 | 14.3 | 105.9 | NA | NA | NA |
| V4 | 926 | 3.5 | 1412 | 471 | 12.5 | 130.0 | 48.3 | 29.6 | 4.1 |
| V5 | 730 | 6.0 | 1307 | 436 | 11.6 | 111.5 | 43.7 | 26.2 | 3.5 |
| V6 | 105 | 0.5 | 159 | 53 | 1.7 | 15.0 | 4.8 | 7.8 | 0.7 |
| V7 | 25 | 0.6 | 40 | 13 | 1.1 | 3.5 | 1.8 | NA | NA |
| V8 | 56 | 4.0 | 92 | 31 | 4.3 | 10.8 | 4.4 | 3.5 | 0.8 |
| V9 | 73 | 0.5 | 138 | 46 | 1.9 | 9.5 | 5.6 | 3.4 | 1.0 |
| V10 | 37 | 0.9 | 61 | 20 | 1.0 | 2.4 | 1.2 | NA | NA |
| V11 | 91 | 1.0 | 164 | 55 | 1.7 | 12.8 | 6.0 | 3.3 | NA |
| V12 | 48 | 0.3 | 13 | 4 | 0.9 | NA | NA | NA | NA |
| V13 | 248 | 0.3 | 512 | 171 | 2.9 | 43.3 | 15.8 | 10.8 | 1.9 |
| V14 | 513 | 0.5 | 1010 | 337 | 6.5 | 86.1 | 33.4 | 20.1 | 2.8 |
| V15 | 100 | 1.5 | 213 | 71 | 3.0 | 19.3 | 7.3 | 3.3 | NA |
| V16 | 6 | 0.1 | 17 | 6 | 1.3 | 0.9 | NA | NA | NA |
| V17 | 46 | 0.2 | 84 | 28 | 112.0 | 26.8 | 5.4 | 2.0 | NA |
| V18 | 273 | 0.2 | 601 | 201 | 5.4 | 52.8 | 17.9 | 9.3 | 1.7 |
| V19 | 561 | 0.5 | 1236 | 412 | 10.0 | 100.7 | 36.4 | 20.8 | 2.4 |
| V20 | 98 | 4.6 | 210 | 70 | 0.2 | 20.5 | 7.6 | NA | NA |
| V21 | 18 | 1.2 | 42 | 14 | 5.6 | 4.1 | 2.3 | NA | NA |
| 2[D43 matrix | | | | | | | | | |
| M1 | | 5 | NA | NA | 0.9 | 11.2 | NA | NA | NA |
| M2 | | 5 | NA | NA | 1.3 | 2.1 | NA | NA | NA |
| M3 | | 2 | NA | NA | 2.4 | 5.7 | NA | NA | NA |
| M4 | | 2 | NA | NA | 1.4 | 1.3 | NA | NA | NA |
| M5 | | 2 | NA | NA | 1.1 | 5.4 | NA | NA | NA |

Abundances for laser shots on the matrix are also reported. All 1-sigma uncertainties are of 10%. CO_2 concentration is estimated assuming a constant $^4\text{He}/^3\text{He}$ of 90,000 and the $\text{CO}_2/^3\text{He}$ of 2.7×10^9 measured on the same sample by Javoy and Pineau (1991).

Table 2
He, Ne and Ar isotopic compositions from laser extraction of single vesicle of “Popping rock” 2[D43

| | $^3\text{He}/^4\text{He}$ | R/Ra | $^{20}\text{Ne}/^{22}\text{Ne}$ | $^{21}\text{Ne}/^{22}\text{Ne}$ | $^{40}\text{Ar}/^{36}\text{Ar}$ | $^{38}\text{Ar}/^{36}\text{Ar}$ | $^4\text{He}/^{40}\text{Ar}^*$ |
|----------------------|---------------------------|-------------|---------------------------------|---------------------------------|---------------------------------|---------------------------------|--------------------------------|
| <i>2[D43 vesicle</i> | | | | | | | |
| V1 | 92,470 (7890) | 7.81 (0.67) | 10.46 (0.55) | 0.027 (10) | 6260 (220) | 0.185 (4) | 1.26 (6) |
| V2 | 92,070 (3580) | 7.85 (0.31) | 11.80 (1.99) | 0.067 (37) | 22,570 (870) | 0.182 (4) | 1.35 (7) |
| V3 | 88,430 (2420) | 8.17 (0.22) | 11.75 (0.50) | 0.050 (7) | 27,780 (800) | 0.184 (1) | 1.31 (6) |
| V4 | 93,190 (1880) | 7.75 (0.16) | 11.80 (0.20) | 0.054 (3) | 27,870 (740) | 0.189 (1) | 1.34 (7) |
| V5 | 90,020 (1940) | 8.03 (0.17) | 12.25 (0.28) | 0.058 (4) | 27,070 (710) | 0.188 (1) | 1.48 (7) |
| V6 | 88,370 (6510) | 8.18 (0.60) | 11.50 (0.69) | 0.058 (16) | 28,520 (1,010) | 0.187 (2) | 1.29 (6) |
| V7 | 97,390 (14,570) | 7.42 (1.11) | NA | NA | 27,040 (2,070) | 0.184 (5) | 1.52 (8) |
| V8 | 97,720 (7950) | 7.39 (0.60) | 10.49 (0.27) | 0.038 (6) | 20,740 (770) | 0.189 (3) | 1.44 (7) |
| V9 | 86,810 (4900) | 8.32 (0.47) | 11.34 (0.67) | 0.034 (13) | 36,470 (1,350) | 0.188 (4) | 1.41 (7) |
| V10 | 102,560 (11,650) | 7.05 (0.80) | 11.08 (1.21) | 0.050 (25) | NA | NA | NA |
| V11 | 93,720 (3770) | 7.71 (0.31) | 11.65 (1.11) | 0.060 (18) | 30,850 (1,150) | 0.188 (3) | 1.45 (7) |
| V12 | 135,240 (54,960) | 5.34 (2.17) | NA | NA | NA | NA | NA |
| V13 | 86,170 (3440) | 8.39 (0.34) | 11.66 (0.62) | 0.065 (12) | 28,890 (430) | 0.190 (2) | 1.51 (8) |
| V14 | 88,420 (3120) | 8.17 (0.29) | 11.96 (0.37) | 0.056 (16) | 29,710 (260) | 0.192 (1) | 1.48 (7) |
| V15 | 85,710 (3680) | 8.43 (0.36) | 11.86 (0.49) | 0.034 (8) | 26,700 (570) | 0.190 (1) | 1.51 (8) |
| V16 | 94,720 (17,640) | 7.63 (1.42) | NA | NA | NA | NA | NA |
| V17 | 91,540 (4870) | 7.89 (0.42) | 9.99 (0.17) | 0.033 (2) | 11,510 (210) | 0.186 (2) | 0.99 (5) |
| V18 | 86,340 (3546) | 8.37 (0.34) | 11.44 (0.28) | 0.053 (5) | 26,610 (370) | 0.189 (1) | 1.54 (7) |
| V19 | 88,330 (2940) | 8.18 (0.27) | 11.92 (0.25) | 0.060 (5) | 28,030 (280) | 0.189 (1) | 1.57 (8) |
| V20 | 90,750 (3807) | 7.96 (0.33) | NA | NA | 25,850 (560) | 0.187 (2) | 1.41 (7) |
| V21 | 91,110 (6490) | 7.93 (0.56) | 10.31 (0.29) | 0.029 (4) | 21,770 (1,890) | 0.179 (7) | 1.56 (8) |
| <i>2[D43 matrix</i> | | | | | | | |
| M1 | NA | NA | 9.91 (1.3) | NA | 306 (10) | 0.180 (4) | NA |
| M2 | NA | NA | 10.15 (0.8) | NA | 331 (18) | 0.172 (15) | NA |
| M3 | NA | NA | 11.67 (2.2) | NA | 310 (14) | 0.194 (7) | NA |
| M4 | NA | NA | 9.05 (1.83) | NA | 258 (43) | 0.182 (18) | NA |
| M5 | NA | NA | 8.80 (1.02) | NA | 199 (94) | 0.208 (27) | NA |

R/Ra is the $^3\text{He}/^4\text{He}$ ratio normalized to the air ratio (1.384×10^{-6}). All data are corrected for blank. An additional correction has been included for the pressure effect on the mass discrimination for $^{38}\text{Ar}/^{36}\text{Ar}$ and $^{40}\text{Ar}/^{36}\text{Ar}$ ratio. Analyses of matrix are also reported, showing an air-like isotopic composition. All isotopic data are given with 1σ uncertainty. NA means not available values generally due to the signal being indistinguishable from the blank.

atmospheric $^3\text{He}/^4\text{He}$ with a value of 1.384×10^{-6} . The average decreases to $90,000 \pm 3000$ (or 8.03 ± 0.28) if data with uncertainties more than 10% are not considered. This value is similar to the value reported by crushing (Fig. 2).

^{36}Ar abundances in an individual vesicle vary between 1×10^{-13} and 1.3×10^{-11} cm^3STP . In the majority of cases, the proportion of blank does not exceed 50% of the signal of the vesicle. However, some abundances were too low to be measurable.

Argon isotopic ratios are reported in a $^{40}\text{Ar}/^{36}\text{Ar}$ versus $^3\text{He}/^{36}\text{Ar}$ diagram (Fig. 3). Data, where the analytical uncertainty on $^{40}\text{Ar}/^{36}\text{Ar}$ ratios is higher than 10% (1σ uncertainties) are not reported, because

they correspond to a high blank correction (>90%). For comparison, the data obtained by step crushing from Kunz (1999), Moreira et al. (1998), and Raquin and Moreira (2005) are also plotted. The $^{40}\text{Ar}/^{36}\text{Ar}$ ratio of single vesicles varies between 6300 and 36,500. However, what is very surprising is that 2/3 of the data shows a $^{40}\text{Ar}/^{36}\text{Ar}$ between 27,000 and 30,000. These ratios are similar to the highest values obtained by crushing, with the exception of seven points labeled individually on Fig. 3. Six of these points have lower $^{40}\text{Ar}/^{36}\text{Ar}$ ratios between 6300 and 22,500, while V9 has a higher ratio of $36,470 \pm 1350$ (1σ). This latter value

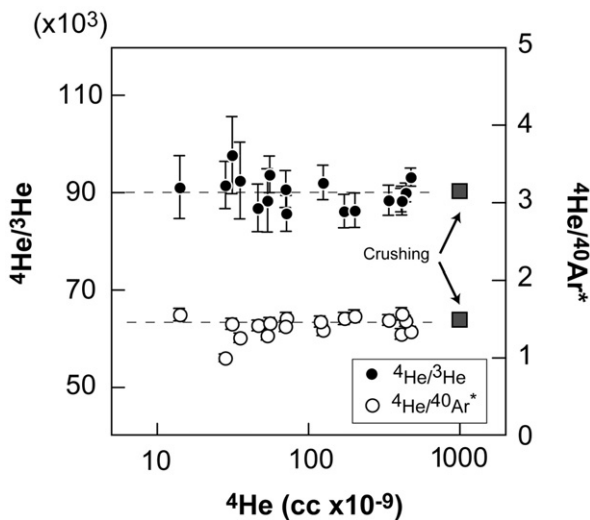


Fig. 2. $^4\text{He}/^3\text{He}$ and $^4\text{He}/^{40}\text{Ar}^*$ ratios in single vesicles of the popping rock 2[D43. Ratios are homogeneous and similar to the ratios obtained by crushing or heating on the same sample (Moreira et al., 1998; Raquin and Moreira, 2005).

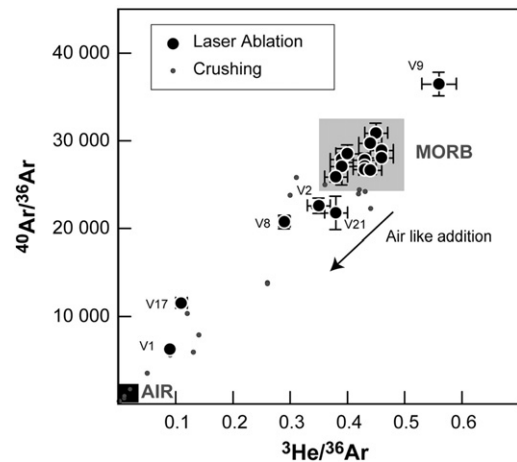


Fig. 3. Data of single vesicles plotted in the $^{40}\text{Ar}/^{36}\text{Ar}$ ratio versus the $^3\text{He}/^{36}\text{Ar}$ ratio diagram. Data from Moreira et al. (1998) and Raquin and Moreira (2005), obtained by crushing, are also reported. Data on single vesicle do not spread over the mixing line obtained by crushing. Most of the data, not labeled, have a mantle-like isotopic composition with a $^{40}\text{Ar}/^{36}\text{Ar}$ ratio similar to the highest values obtained by crushing. Only a few vesicles, shown by their labels, have a different $^{40}\text{Ar}/^{36}\text{Ar}$ and $^3\text{He}/^{36}\text{Ar}$ ratios. Except for the vesicle V9, the isotopic ratios are lower, which can be the result of a little contribution of gases released from the ablated matrix, with atmospheric composition.

is close to the mean $^{40}\text{Ar}/^{36}\text{Ar}$ of the plateau observed (in a $^{40}\text{Ar}/^{36}\text{Ar}$ -1/ ^{36}Ar diagram) for the same popping rock by Burnard et al. (1997). Indeed, this value is 32,440 and probably corresponds to the uncontaminated argon ratio for the sample piece analyzed by Burnard et al. (1997).

Our data are more homogenous than the data of Burnard et al. (1997), where the $^{40}\text{Ar}/^{36}\text{Ar}$ ratio in single vesicles start from 3500 and increase up to 40,000.

The $^{38}\text{Ar}/^{36}\text{Ar}$ is indistinguishable from the atmospheric ratio (0.1880), within uncertainties, even for $^{40}\text{Ar}/^{36}\text{Ar}$ ratios higher than 25,000.

The $^4\text{He}/^{40}\text{Ar}^*$ ratio ($^{40}\text{Ar}^*$ is radiogenic ^{40}Ar , meaning corrected for air) in individual vesicles are also homogeneous, with a mean value of 1.41 ± 0.14 (Fig. 2). This ratio is within uncertainty identical to that obtained by crushing (1.5) (Moreira et al., 1998; Raquin and Moreira, 2005).

^{22}Ne abundances in single vesicles vary between 10^{-13} cm³ and 1.4×10^{-12} cm³. As the blank signal reaches 95% of the analyzed signal released from a single vesicle, $^{20}\text{Ne}/^{22}\text{Ne}$ isotopic ratios have uncertainties ranging from 2% to 20%. For neon isotopes, we have discarded data with $1\sigma > 10\%$ (data corresponding to more than 90% of blank). In spite of the large uncertainty, a detectable signature is revealed. The neon data are reported in the three-neon isotopes diagram. The $^{20}\text{Ne}/^{22}\text{Ne}$ varies between 10.31 ± 0.29 and 12.25 ± 0.28 , with most of the data having a $^{20}\text{Ne}/^{22}\text{Ne}$ ratio above 11.5, with an average value of 11.7 ± 0.3 . Vesicles showing the slightly smaller ratios have been distinguished from other samples in Fig. 4. They are associated to low abundances, with the exception of the vesicle V17, which has the highest amount of ^{22}Ne (10^{-11} cm³).

Within uncertainty, the neon data are similar to the highest values obtained by step crushing (considered to be the mantle signature) (Sarda et al., 1988; Moreira et al., 1998; Raquin and Moreira, 2005). They plot very close to the neon-B ratio (12.5) and clearly different to the solar wind value (13.8).

^{84}Kr abundance varies between 4.8×10^{-13} and 4.8×10^{-15} cm³STP. ^{129}Xe abundance varies between 2×10^{-15} and 3×10^{-14} whereas ^{130}Xe is less than 5×10^{-15} cm³STP.

CO_2 abundances were estimated using the $\text{CO}_2/{}^3\text{He}$ ratio of 2.7×10^9 reported by Javoy and Pineau (1991) and the mean value of

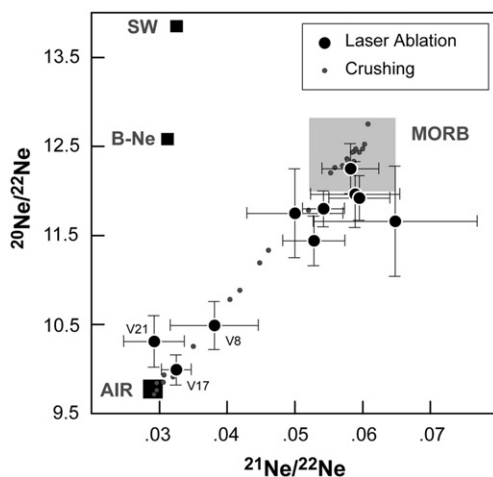


Fig. 4. Neon data for single vesicles in the three-neon isotope diagram. Data from Kunz (1999), Moreira et al. (1998) and Raquin and Moreira (2005) obtained by crushing are also reported. The shaded box defines the uncontaminated MORB domain (focused on a $^{20}\text{Ne}/^{22}\text{Ne}$ value of 12.5 with an associated $^{21}\text{Ne}/^{22}\text{Ne}$ ratio of 0.06) (Moreira et al., 1998). According to the uncertainties and except some labeled vesicles, the $^{20}\text{Ne}/^{22}\text{Ne}$ ratio of single vesicles of popping rock is similar to the highest values obtained by crushing. This value is close to the neon-B value (12.5). The poor-gas labeled vesicles V21 and V8 have lower $^{20}\text{Ne}/^{22}\text{Ne}$, which tend to atmospheric values, consistent with a contribution of gases released from the ablated matrix.

the $^4\text{He}/{}^3\text{He}$ of the vesicles (90,000). The CO_2 varies between 1.5×10^{-4} and 1.4×10^{-2} cm³ (or 6 and 630 nmol). We note that the lowest amount of gases recorded during this study are similar to the highest abundances reported by Burnard et al. (1997) on the same sample, but on a 300 μm thick section. The importance of sample thickness, hence vesicle size is discussed later in the present study.

Two vesicles (V1 and V17) present elemental composition slightly different from the other vesicles. According to their CO_2 (or ^4He) abundances, they have an exceptionally high amount of Ne or Ar. Those vesicles present the lowest argon isotopic ratio too, trending to an air-like value (e.g. $^{40}\text{Ar}/^{36}\text{Ar}$ of 6260 ± 220 and $11,510 \pm 210$ respectively). They are reminiscent of the air component seen during crushing or heating experiment but the amount of gases released is not as abundant as it would be expected. Moreover, the vesicle V17 has 10 times more ^{22}Ne than the other vesicles and this enrichment is not observed with the ^{36}Ar . We do not have explanation for such a behavior. This leads us to take this data point carefully.

4. Discussion

4.1. The $^4\text{He}/^{40}\text{Ar}^*$ ratio

The $^4\text{He}/^{40}\text{Ar}^*$ ratio measured in single vesicle is very homogeneous (1.5) and identical to the ratio measured during crushing (1.5) experiment. Such homogeneity was previously seen by Burnard and collaborators even if they measured a $^4\text{He}/^{40}\text{Ar}^*$ ratio slightly lower (0.99) (Burnard et al., 1997). The constancy in the $^4\text{He}/^{40}\text{Ar}^*$ ratio is in agreement with the study of Sarda and Graham (1990) on this sample, when they claim that this sample has only a single population of vesicles and that the use of this sample is appropriated to constrain models of vesiculation (Guillot and Sarda, 2006).

As mentioned above, there is a difference between the $^4\text{He}/^{40}\text{Ar}^*$ measured in this study (1.5) and the one measured by Burnard and collaborators (0.99). This difference could be due to different degrees of magmatic degassing between vesicles. All Chunks used in the present study had a vesicularity visually estimated between 15 and 20%. This is higher than the vesicularity of the pieces of sample analyzed by Burnard et al. (1997) (5%). This could reflect a greater degree of exsolution. The majority of helium and argon is in the gas phase, with minimum levels of gases still remaining in the glass. In our study, several pieces of sample were used and it is highly unlikely that each individual piece of sample has exactly the same vesicularity. Despite this, the $^4\text{He}/^{40}\text{Ar}^*$ ratio in each vesicle is identical.

It is also important not to neglect the potential for variation of the mass discrimination or sensitivity during analysis at low pressure. Hence, an alternative explanation is that the difference between our results and those of Burnard et al. (1997) is due to an analytical artifact because their study, argon isotopic ratio was not corrected for the mass discrimination related to the amount of gases introduced in the mass spectrometer (Burnard personal communication). This lack of correction could reconcile the lower $^4\text{He}/^{40}\text{Ar}^*$ ratio and the more dispersed $^{40}\text{Ar}/^{36}\text{Ar}$ ratio in their data set. Indeed, without the mass discrimination correction applied to our data set, we would overestimate the $^{40}\text{Ar}/^{36}\text{Ar}$ ratio by about 3%. That would have induced an overestimate of the $^{40}\text{Ar}^*$ and then an underestimate of the $^4\text{He}/^{40}\text{Ar}^*$.

The value of 1.5 for the $^4\text{He}/^{40}\text{Ar}^*$ ratio is the lowest measured in MORB samples. It coincides with the ratio expected for the mantle from estimated K and U concentrations (Allègre et al., 1987). For the vesicularity observed on the popping rock (>10%), due to the low solubility of rare gases in melts, all of them are located in vesicles. This implies that noble gases have been transferred entirely to the vesicle and that the amount of gases left in the glass is negligible. As a consequence there should be minimal or no elemental fractionation during melting process, which tend to strengthen the view that the noble gases are incompatible elements (Brooker et al., 2003; Heber et al., 2007).

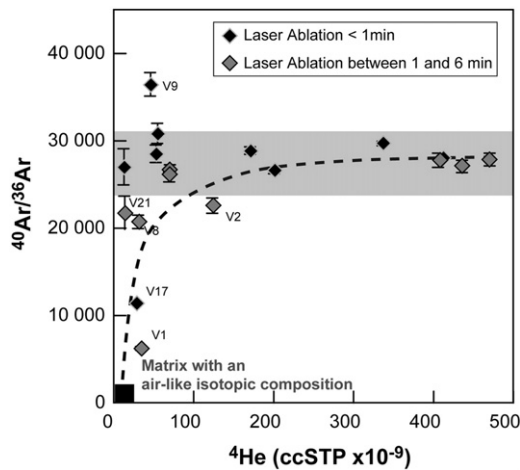


Fig. 5. Effect of gases released from the matrix on the signal of the vesicles according to the time of ablation and the vesicle gas contents. For gas-poor vesicle (with a ^4He abundance less than $2 \times 10^{-7} \text{ cm}^3\text{STP}$) and long time of laser ablation, the signal of the matrix perturbs the signal of the vesicle (dashed line). For the other cases, the $^{40}\text{Ar}/^{36}\text{Ar}$ recorded in single vesicle is constant with a mean value of $27,000 \pm 4000$. This indicates that only one population of vesicles is pierced with a mantle composition.

4.2. Isotopic compositions

The Ne–Ar systematics show that the majority of the vesicles have isotopic compositions very close to the highest values obtained by step crushing and heating experiments on the same sample (12.5 and 25,000) (Kunz, 1999; Moreira et al., 1998; Raquin and Moreira, 2005). However, in the case of argon, vesicles V1, V2, V8, V9, V17, V21 (for neon, only V8, V17, V21 are reported) have slightly different ratios and, except V9, closer to an atmospheric end-member.

Compositions from those vesicles seem to define a mixture between the mantle signature and an air-like component. Nevertheless, this mixture is different from that obtained during the crushing or heating experiments. During the crushing or heating procedure, rare gases have a “pure” atmospheric signature with $^{40}\text{Ar}/^{36}\text{Ar}$ ratio equal to 296 and $^{20}\text{Ne}/^{22}\text{Ne}$ equal to 9.8, in the first steps. Concentrations associated to these values are up to three orders of magnitude higher than concentrations associated to mantle values (Kunz, 1999; Moreira et al., 1998; Staudacher et al., 1989; Raquin and Moreira, 2005; Sarda et al., 1988).

The basaltic matrix pulverized by ablation can contain gases, which can be added to the signal of vesicles. Two possible sources of gases can be released from the matrix: 1 – gases adsorbed on the surface of the sample at the point of impact, and 2 – gases dissolved in the volume of the ablated matrix.

To test the contribution from these two sources of gas, two factors must be taken into account. The first is the time of ablation before piercing a vesicle, which is proportional to the volume of the pulverized matrix. The second factor is the rare gases amount released from the vesicle. The lower the amount of rare gases in the vesicle, the greater the degree of contamination from the matrix. The influence of the matrix on the signal of the vesicle is observed in the $^{40}\text{Ar}/^{36}\text{Ar}$ versus ^4He abundances diagram (Fig. 5). Data are plotted with different symbols according to the time of ablation. The matrix was initially analyzed. Its signature clearly differs from the mantle composition in spite of the large uncertainties and shows an air-like isotopic composition. The helium abundance was below the detection limit, indistinguishable from the blank.

The $^{40}\text{Ar}/^{36}\text{Ar}$ ratio is constant ($27,000 \pm 4000$) for either high gas abundances with long time of ablation ($> 1 \text{ min}$) or short time of ablation ($< 1 \text{ min}$) with high or low rare gas abundances. A matrix contribution can be observed for long ablation times, associated with low amount of gases. Vesicles named for their low $^{20}\text{Ne}/^{22}\text{Ne}$ and $^{40}\text{Ar}/^{36}\text{Ar}$ ratios and

presenting both long time laser ablation and low amount of gases. A small influence of volatiles released from the matrix explains their “non-mantle” signature. The tendency of this influence is underlined by the dashed curve on Fig. 5. If gases released from such a small volume of matrix can induce isotopic variations during laser ablation, then during crushing or heating experiment, a much greater volume of gas with this air-like signature must be released, causing the mixing line generally observed. Indeed, during crushing, new surfaces are exposed to vacuum. This may encourage degassing by the direct application of the Henry's law. Moreover, diffusion is also encouraged because during crushing, the sample can be heated at temperatures above 50°C .

This is evident in the $^{40}\text{Ar}/^{36}\text{Ar}$ versus $^{20}\text{Ne}/^{22}\text{Ne}$ space (Fig. 6). Data obtained by crushing from Kunz (1999), Moreira et al. (1998), and Raquin and Moreira (2005) are also plotted alongside the ablation data from the present study. In such a diagram, a mixture between two components is defined by a mixing hyperbola where the R parameter reflects the $(^{36}\text{Ar}/^{22}\text{Ne})_{\text{air}}/(^{36}\text{Ar}/^{22}\text{Ne})_{\text{mantle}}$ ratio. Data obtained using the laser ablation system and those obtained by crushing plot on two different hyperbolae. Hence, there are two air-like components with two different $^{36}\text{Ar}/^{22}\text{Ne}$ ratios in the basalt.

The first is the one released during crushing experiment (not seen during the laser ablation procedure). The mixing hyperbola fitting the best data obtained by crushing, for a neon-B $^{20}\text{Ne}/^{22}\text{Ne}$ ratio (12.5) and $^{40}\text{Ar}/^{36}\text{Ar}$ of 27,000, is achieved for a R parameter of 1.6. Taking the value of 12.25 for the $^{36}\text{Ar}/^{22}\text{Ne}$ ratio in the upper mantle (Moreira et al., 1998) this first air-like component has a $^{36}\text{Ar}/^{22}\text{Ne}$ ratio of around 19, which is exactly the atmospheric value. Note that this ratio can be also obtained when air (with a $^{36}\text{Ar}/^{22}\text{Ne}$ of 18.7; Ozima and Podosek, 1983) is first dissolved in seawater (it increases to 71; Allègre et al., 1987) and then when that seawater is dissolved into magma (the ratio comes back to 18.7). The solubility in seawater and basalts compensate each other numerically.

The second air-like component is the one released from the matrix during laser ablation. In this case, the mixing hyperbola fitting the best the data (except V9) is achieved for a R parameter of 0.1 (Fig. 6). The calculated $^{36}\text{Ar}/^{22}\text{Ne}$ ratio of the matrix (for $^{36}\text{Ar}/^{22}\text{Ne}$ ratio of 12.25 the upper mantle) is then 1.2. This value is close to the mean $^{36}\text{Ar}/^{22}\text{Ne}$ measured in the matrix sample (4 ± 3) (Table 1).

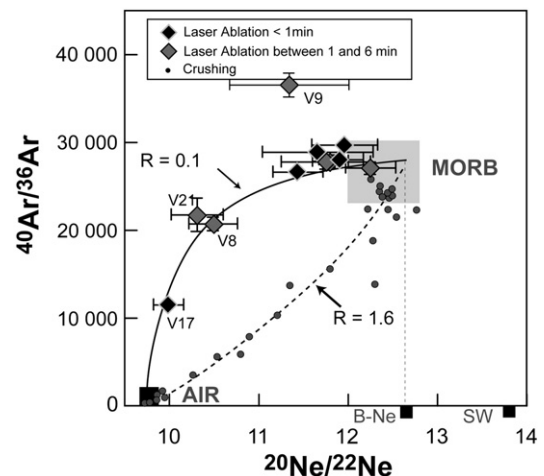


Fig. 6. $^{20}\text{Ne}/^{22}\text{Ne}$ versus $^{40}\text{Ar}/^{36}\text{Ar}$. Data obtained by laser ablation on a different mixing hyperbola than those obtained by crushing (Kunz, 1999; Moreira et al., 1998; Raquin and Moreira, 2005). R is a parameter defining the curvature of the two different mixing hyperbolae ($= (^{36}\text{Ar}/^{22}\text{Ne})_{\text{air-like}}/(^{36}\text{Ar}/^{22}\text{Ne})_{\text{mantle}}$). Data obtained using the laser air-like mantle ablation method (except V9) plot on a mixing hyperbola defined with $R=0.1$ whereas data obtained using crushing plot on a mixing hyperbola with $R=1.6$. This indicates that the $^{36}\text{Ar}/^{22}\text{Ne}$ of the matrix is different from the $^{36}\text{Ar}/^{22}\text{Ne}$ of the very abundant air-like component released by crushing. Consequently, there are 3 components in the glass: the matrix, the mantle component and the air-like component, not seen in this study.

One way to produce the $^{36}\text{Ar}/^{22}\text{Ne}$ in the matrix is to dissolve first seawater in magma. As described above the resulting $^{36}\text{Ar}/^{22}\text{Ne}$ ratio will be 18.7. Secondly, this magma is degassed. According to the solubility of neon and argon from Jambon et al. (1986), the residue in the matrix will have a $^{36}\text{Ar}/^{22}\text{Ne}$ ratio of ~ 4 , close to our calculated $^{36}\text{Ar}/^{22}\text{Ne}$ ratio in the matrix (1.2) or our measured value (4 ± 3).

Another possible process that can provide the $^{36}\text{Ar}/^{22}\text{Ne}$ ratio measured in the matrix is solution of noble gases from seawater or from air in rigid glass after cooling on the sea floor into the first nanometers of the glass rim. Because neon has a higher solubility than argon in silicate glasses, it can conduct to a smaller $^{36}\text{Ar}/^{22}\text{Ne}$ ratio (<5).

The main conclusions on the study of the signal of the matrix are the following:

1. Using the laser ablation extraction procedure, we have only detected one population of vesicles with a mantle signature ($^{40}\text{Ar}/^{36}\text{Ar} = 27,000 \pm 4000$ and $^{20}\text{Ne}/^{22}\text{Ne} = 11.7 \pm 0.3$). The lower values can be attributed to the contamination of gases released from the matrix.
2. There are three sources of rare gases in this basalt: the mantle-derived component, the matrix, and an air-like component, which is not observed by the ablation procedure but is only present during crushing extraction procedure. The matrix and this air component have two different $^{36}\text{Ar}/^{22}\text{Ne}$ ratios as indicated by the two mixing hyperbolae in Fig. 6.
3. The two hyperbolae describing the mixture between the mantle component and the two air related components (one seen on crushing the other on ablation) can provide constraints on the $^{40}\text{Ar}/^{36}\text{Ar}$ and $^{20}\text{Ne}/^{22}\text{Ne}$ value of the degassed mantle because they have the same mantle end-member in common. Hence, the $^{20}\text{Ne}/^{22}\text{Ne}$ ratio can be considered as close to the Neon-B ratio (12.5) (Black, 1972) and the associated $^{40}\text{Ar}/^{36}\text{Ar}$ ratio as close to 27,000. The small difference between the $^{20}\text{Ne}/^{22}\text{Ne}$ ratio measured in single vesicle (11.7) and that of the Neon-B (12.5) can be due to a small contribution of neon from the matrix even for short time of laser shooting.

4.3. Origin of the air-like component released by crushing

The location of the atmospheric component present in the basalt released by crushing remains unidentified. It has been mentioned that the site bearing the air-like component must be the easier to rupture like the largest vesicles (Ballentine and Barfod, 2000; Sarda, 2004).

In his model, Sarda proposed that such vesicle can be formed in the 2][D43 sample during the melt of a heterogeneous mantle reservoir. This reservoir contains the normal lherzolitic component and a recycled component (with an air-like noble gas signature) (Sarda, 2004). In this model, the recycled component melts preferentially compared to the lherzolitic component and induces the formation of air-bearing vesicles. As the melt occurs, the proportion of the recycled component decreases and let the formation of vesicle with a more normal lherzolitic mantle signature. The first vesicles have more time to grow; hence the air-like component is related to the largest vesicle. As this sample does not suffer of lost of vesicles such heterogeneity in the isotopic signature may be preserved in the vesicles. Then, it is important to have an estimation of the range of the size of the decrepitated vesicle. Unfortunately, in the present study it was not possible to determine the size of the vesicle that was pierced. Indeed, it is not simple to have a 3D cartography on 1 cm^3 samples with a resolution of few microns. However, by comparison our results with the results of studies of Burnard and collaborators and Sarda and Graham on the same sample (Burnard et al., 1997; Sarda and Graham, 1990), we were able to estimate the maximum size of the vesicles that was pierced but it requires some assumptions.

1. In Burnard's work, thin sections of $300\ \mu\text{m}$ have been made in order to have cartography of the vesicle. The largest vesicle that can be pierced

with this sample preparation is $200\ \mu\text{m}$ (see the analytical procedure in Burnard, 1999b). The assumption is that in Burnard's study on the 2][D43 sample (Burnard et al., 1997), the size of the vesicles containing the highest amount of gases corresponds to the largest vesicle that can be pierced with this sample preparation ($200\ \mu\text{m}$). This vesicle is the 4/la7 vesicle, where CO_2 and ^4He abundances are $4 \times 10^{-4}\ \text{cm}^3$ and $1 \times 10^{-8}\ \text{cm}^3$ respectively (on a range of abundance varying between $7 \times 10^{-5}\ \text{cm}^3$ and $4 \times 10^{-4}\ \text{cm}^3$ for CO_2 and associated ^4He amount between $2 \times 10^{-9}\ \text{cm}^3$ and $1 \times 10^{-8}\ \text{cm}^3$).

2. The abundance of the vesicle 4/la7 from is almost similar to the lowest abundances recorded in our present study (vesicle V7 where CO_2 and ^4He are $4 \times 10^{-4}\ \text{cm}^3$ and $1.3 \times 10^{-8}\ \text{cm}^3$ STP). Hence the maximum size of the vesicle V7 can be evaluated at $200\ \mu\text{m}$ in diameter.
3. We consider that all the pierced vesicles (with a mantle composition) had the same pressure prior to the ablation. The vesicle size distribution, well described by Sarda and Graham, implies that the nucleation was done in equilibrium with the surrounding magma with no significant movement of the vesicle compared to the melt and at relatively slow magma ascent rate (Sarda and Graham, 1990). The identical $^4\text{He}/^{40}\text{Ar}^*$ of each vesicle strengthens this hypothesis. Then the pressure of volatiles in vesicles after the rapid quenching of lava can thus be considered to be the final equilibrium pressure at the depth of eruption ($\sim 350\ \text{bar}$).

The pressure in the cell when gases are released from a vesicle is less than 1 Torr. CO_2 , the major gas (more than 90%, Javoy and Pineau, 1991) can be considered as a perfect gas. The ratio of the diameters for two different vesicles is given by the cubic root of the ratio of the pressures measured in the cell: $\frac{D_1}{D_2} = \left(\frac{P_1}{P_2}\right)^{1/3} \approx \left(\frac{n_{\text{CO}_2,1}}{n_{\text{CO}_2,2}}\right)^{1/3}$.

D_1 and D_2 are the diameters of two vesicles Va and Vb, P_1 and P_2 are the pressures recorded in the cell when Va and Vb decrepitated.

$\frac{D_1}{D_2} = 3.3$ when pressures recorded for the vesicles V7 (25 mTorr) and V4 (926 mTorr) are considered. If we assume that vesicle V7 has a diameter of $200\ \mu\text{m}$, vesicles with a diameter less than $660\ \mu\text{m}$ have been pierced.

Studies on vesicle size distribution on centimeter-size sample, similar to the samples we introduced in the cell for this study, show that the observable vesicle size varies between 0.02 and 1.5 mm (Burnard, 1999a; Sarda and Graham, 1990). Hence, we have pierced an intermediate range of this vesicle size distribution. It is easy to imagine that the smaller vesicles were too gas-poor to be detected. If a pierced vesicle of $200\ \mu\text{m}$ in diameter causes an increase of pressure in the cell of 25 mTorr, then a $20\ \mu\text{m}$ vesicle will cause an increase of the pressure of 0.02 mTorr in the cell, one order of magnitude below the detected level (0.1 mTorr). However, largest vesicles with a diameter as great as 1.5 mm were not detected in the present study and a possible reason is the following.

The scarcity of piercing vesicles using a laser beam of some tens of microns in diameter has to be mentioned. The probability to open a vesicle of a given size can be defined as the ratio of the surface area of the vesicles of a given size to the total surface of the sample in two dimensions. Using the vesicle size distribution data from Sarda and Graham for sample one (similar to our chunk of sample, Sarda and Graham, 1990), we are able to estimate the probability to pierce large vesicles. In their paper, 12 vesicle classes have been determined. The largest, (i.e. 1.31 to 1.04 mm) has a mean diameter of 1.18 mm. The surface of one such spherical vesicle is $\pi \times \frac{D^2}{4} = 1.08\ \text{mm}^2$. The measured number of such vesicle per unit area (mm^2) is 0.0189. Then, the surface fraction occupied by those vesicle is: $1.8 \times 0.0189 = 0.02$. The probability of opening the largest class of vesicle is 2%. Doing the same calculation, for all classes of vesicle, we demonstrate that the probability of shooting open a vesicle of a given size does not exceed 2.5% (for the intermediate class: i.e. 0.52 to 0.66 mm). The scarcity to shoot open a large vesicle can explain why we have not seen vesicle as large as 1.5 mm of diameter.

The maximum depth at which the laser can penetrate into the matrix can also be a parameter that increases the scarcity of having

large vesicles. For one-minute shot, the depth of the crater is around 70 μm . For the maximum laser time (6 min) the depth of the crater becomes 150 μm . Therefore, some vesicles that were located too close to the surface of the sample could have been previously opened. Other vesicles may be positioned too deep to be reached by the laser beam. Moreover, for vesicle ideally positioned, the thickness of the glass separating the pressurized vesicle from the outside can be too fragile to withstand the pumping of the cell after the sample is placed.

Given the small penetration depth and the low probability of opening a vesicle, the possibility still exists that large vesicle (1.5 mm of diameter) has not been seen in this study.

This size of 660 μm for the largest decrepitated vesicle in this study is a maximum estimation. Nevertheless, all the vesicles with high gas concentrations then considered as the biggest decrepitated vesicle in this study (except the vesicle V17), have almost the same mantle isotopic composition. There is no continuous range of vesicle composition according to the size of the vesicle as the model where vesicles were formed from two different material sources (recycled and primordial) predicted (Sarda, 2004).

Another possibility, which may be the overwhelming atmospheric component measured in oceanic basalts during crushing or heating experiment is that the site bearing this component is not the largest vesicles of samples but some cracks as suggested by Ballentine and Barfod (2000). However, the mechanism for the incorporation of the atmospheric component into the basalt remains unknown.

5. Conclusions

For the first time, both elemental and isotopic compositions of He, Ne and Ar in single vesicles of MORB have been measured. The $^4\text{He}/^3\text{He}$ and $^4\text{He}/^{40}\text{Ar}^*$ ratios are constant and similar to the ratio obtained by crushing experiments. The Ne–Ar systematics indicate that only one population of vesicles with mantle isotopic composition has been pierced with a mean $^{40}\text{Ar}/^{36}\text{Ar}$ value of $27,000 \pm 4000$ and a $^{20}\text{Ne}/^{22}\text{Ne}$ of 11.7 ± 0.3 . The latter value more likely reflects neon-B (12.5) than the Solar wind value (13.8). The two defined mixing hyperbolae indicate that there are three components in the basalt: the mantle component, the matrix and an air-like component not visible in this study, but present during crushing or heating experiments. Gases released from the matrix have an air-like isotopic composition but a $^{36}\text{Ar}/^{22}\text{Ne}$ different to that of the air. Comparisons with the works of Burnard et al. (1997) and Sarda and Graham (1990) imply that the maximum size of decrepitated vesicle in the present study is 660 μm . The largest vesicle has been missed, but according to the very homogeneous composition of vesicles bearing the largest amount of gases in our study, we prefer the model where air-like component always released by crushing is located in some crack as proposed Ballentine and Barfod (2000) rather than the model of recycling proposed by Sarda (2004). However, the exact location of this component still remains unknown.

Acknowledgments

The authors greatly acknowledge Ed. Tipper for helpful discussion. Philippe Sarda and the anonymous reviewer are thanked for their helpful reviews. This paper is dedicated to Jean Marcoux. This is IPGP contribution number 2401.

References

- Allègre, C.J., Moreira, M., 2004. Rare gas systematics and the origin of oceanic islands: the key role of entrainment at the 670 km boundary layer. *Earth and Planetary Science Letters* 228, 85–92.
- Allègre, C.J., Staudacher, T., Sarda, P., Kurz, M., 1983. Constraints on evolution of Earth's mantle from rare-gas systematics. *Nature* 303, 762–766.
- Allègre, C.J., Staudacher, T., Sarda, P., 1987. Rare-gas systematics – formation of the atmosphere, evolution and structure of the Earth's mantle. *Earth and Planetary Science Letters* 81, 127–150.
- Bach, W., Niedermann, S., 1998. Atmospheric noble gases in volcanic glasses from the southern Lau Basin: origin from the subducting slab? *Earth and Planetary Science Letters* 160, 297–309.
- Ballentine, C.J., Barfod, D.N., 2000. The origin of air-like noble gases in MORB and OIB. *Earth and Planetary Science Letters* 180, 39–48.
- Ballentine, C.J., Marty, B., Lollar, B.S., Cassidy, M., 2005. Neon isotopes constrain convection and volatile origin in the Earth's mantle. *Nature* 433, 33–38.
- Black, D.C., 1972. On the origins of trapped helium, neon and argon isotopic variations in meteorites—II. Carbonaceous chondrites. *Geochimica Et Cosmochimica Acta* 36.
- Bougault, H., Dmitriev, L., Schilling, J.G., Sobolev, A., Joron, J.L., Needham, H.D., 1988. Mantle heterogeneity from trace-elements – MAR triple junction near 14-degrees-N. *Earth and Planetary Science Letters* 88, 27–36.
- Brooker, R.A., Du, Z., Blundy, J.D., Kelley, S.P., Allan, N.L., Wood, B.J., Chamorro, E.M., Wartho, J.A., Purton, J.A., 2003. The 'zero charge' partitioning behaviour of noble gases during mantle melting. *Nature* 423, 738–741.
- Burnard, P., 1999a. Eruption dynamics of "popping rock" from vesicle morphologies. *Journal of Volcanology and Geothermal Research* 92, 247–258.
- Burnard, P., 1999b. The bubble-by-bubble volatile evolution of two mid-ocean ridge basalts. *Earth and Planetary Science Letters* 174, 199–211.
- Burnard, P., Graham, D., Turner, G., 1997. Vesicle-specific noble gas analyses of "popping rock": implications for primordial noble gases in earth. *Science* 276, 568–571.
- Farley, K.A., Poreda, R.J., 1993. Mantle neon and atmospheric contamination. *Earth and Planetary Science Letters* 114, 325–339.
- Fisher, D.E., 1997. Helium, argon, and xenon in crushed and melted MORB. *Geochimica Et Cosmochimica Acta* 61, 3003–3012.
- Geertsen, C., Briand, A., Chartier, F., Lacour, J.L., Mauchien, P., Sjöström, S., Mermet, J.M., 1994. Comparison between infrared and ultraviolet-laser ablation at atmospheric pressure – implications for solid sampling inductively-coupled plasma spectrometry. *Journal of Analytical Atomic Spectrometry* 9, 17–22.
- Grimberg, A., Baur, H., Bochsler, P., Buhler, F., Burnett, D.S., Hays, C.C., Heber, V.S., Jurewicz, A.J.G., Wieler, R., 2006. Solar wind neon from Genesis: implications for the lunar noble gas record. *Science* 314, 1133–1135.
- Guillot, B., Sarda, P., 2006. The effect of compression on noble gas solubility in silicate melts and consequences for degassing at mid-ocean ridges. *Geochimica Et Cosmochimica Acta* 70, 1215–1230.
- Harper, C.L., Jacobsen, S.B., 1996. Noble gases and Earth's accretion. *Science* 273, 1814–1818.
- Harrison, D., Burnard, P., Turner, G., 1999. Noble gas behaviour and composition in the mantle: constraints from the Iceland Plume. *Earth and Planetary Science Letters* 171, 199–207.
- Hayashi, C., Nakazawa, K., Mizuno, H., 1979. Earths melting due to the blanketing effect of the primordial dense atmosphere. *Earth and Planetary Science Letters* 43, 22–28.
- Heber, V.S., Brooker, R.A., Kelley, S.P., Wood, B.J., 2007. Crystal–melt partitioning of noble gases (helium, neon, argon, krypton, and xenon) for olivine and clinopyroxene. *Geochimica Et Cosmochimica Acta* 71, 1041–1061.
- Hiyagon, H., Ozima, M., Marty, B., Zashu, S., Sakai, H., 1992. Noble-gases in submarine glasses from midoceanic ridges and Loihi seamount – constraints on the early history of the Earth. *Geochimica Et Cosmochimica Acta* 56, 1301–1316.
- Holland, G., Ballentine, C.J., 2006. Seawater subduction controls the heavy noble gas composition of the mantle. *Nature* 441, 186–191.
- Jambon, A., Weber, H., Braun, O., 1986. Solubility of He, Ne, Ar, Kr and Xe in a basalt melt in the range 1250–1600-degrees-C. *Geochimica Et Cosmochimica Acta* 50, 401–408.
- Javoy, M., Pineau, F., 1991. The volatiles record of a popping rock from the mid-atlantic ridge at 14-degrees-N – chemical and isotopic composition of gas trapped in the vesicles. *Earth and Planetary Science Letters* 107, 598–611.
- Kellogg, L.H., Wasserburg, G.J., 1990. The role of plumes in mantle helium fluxes. *Earth and Planetary Science Letters* 99, 276–289.
- Kunz, J., 1999. Is there solar argon in the Earth's mantle? *Nature* 399, 649–650.
- Marty, B., Zashu, S., Ozima, M., 1983. 2 noble-gas components in a mid-atlantic ridge basalt. *Nature* 302, 238–240.
- Marty, B., Tolstikhin, I.N., 1998. CO₂ fluxes from mid-ocean ridges, arcs and plumes. *Chemical Geology* 145, 233–248.
- Matsumoto, T., Chen, Y.L., Matsuda, J., 2001. Concomitant occurrence of primordial and recycled noble gases in the Earth's mantle. *Earth and Planetary Science Letters* 185, 35–47.
- Mizuno, H., Nakazawa, K., Hayashi, C., 1980. Dissolution of the primordial rare-gases into the molten Earths material. *Earth and Planetary Science Letters* 50, 202–210.
- Moreira, M., Kunz, J., Allègre, C., 1998. Rare gas systematics in popping rock: Isotopic and elemental compositions in the upper mantle. *Science* 279, 1178–1181.
- Mungall, J.E., Bagdassarov, N.S., Romano, C., Dingwell, D.B., 1996. Numerical modelling of stress generation and microfracturing of vesicle walls in glassy rocks. *Journal of Volcanology and Geothermal Research* 73, 33–46.
- Onions, R.K., Tolstikhin, I.N., 1996. Limits on the mass flux between lower and upper mantle and stability of layering. *Earth and Planetary Science Letters* 139, 213–222.
- Ozima, M., Zahnle, K., 1993. Mantle degassing and atmospheric evolution – noble-gas view. *Geochemical Journal* 27, 185–200.
- Patterson, D.B., Honda, M., McDougall, I., 1990. Atmospheric contamination – a possible source for heavy noble-gases in basalts from Loihi Seamount. *Hawaii Geophysical Research Letters* 17, 705–708.
- Pineau, F., Javoy, M., 1994. Strong degassing at ridge crests – the behavior of dissolved carbon and water in basalt glasses at 14-degrees-N, mid-atlantic ridge. *Earth and Planetary Science Letters* 123, 179–198.
- Porcelli, D., Wasserburg, G.J., 1995. Mass-transfer of helium, neon, argon, and xenon through a steady-state upper-mantle. *Geochimica Et Cosmochimica Acta* 59, 4921–4937.
- Porcelli, D., Woolson, D., Cassen, P., 2001. Deep Earth rare gases: initial inventories, capture from the solar nebula, and losses during Moon formation. *Earth and Planetary Science Letters* 193, 237–251.

- Poreda, R.J., Farley, K.A., 1992. Rare-gases in Samoan xenoliths. *Earth and Planetary Science Letters* 113, 129–144.
- Raquin, A., Moreira, M., 2005. Air $^{38}\text{Ar}/^{36}\text{Ar}$ in the mantle: implication for the nature of the parent bodies of the Earth. *Eos Trans. AGU* 86 (52), Fall Meeting. Abstract V13C-0559.
- Sarda, P., 2004. Surface noble gas recycling to the terrestrial mantle. *Earth and Planetary Science Letters* 228, 49–63.
- Sarda, P., Graham, D., 1990. Midocean ridge popping rocks — implications for degassing at ridge crests. *Earth and Planetary Science Letters* 97, 268–289.
- Sarda, P., Staudacher, T., Allègre, C.J., 1985. $^{40}\text{Ar}/^{36}\text{Ar}$ in MORB glasses — constraints on atmosphere and mantle evolution. *Earth and Planetary Science Letters* 72, 357–375.
- Sarda, P., Staudacher, T., Allègre, C.J., 1988. Neon isotopes in submarine basalts. *Earth and Planetary Science Letters* 91, 73–88.
- Sarda, P., Moreira, M., Staudacher, T., 1999. Argon–lead isotopic correlation in Mid-Atlantic Ridge basalts. *Science* 283, 666–668.
- Sasaki, S., 1999. Presence of a primary solar-type atmosphere around the earth: evidence of dissolved noble gas. *Planetary and Space Science* 47, 1423–1431.
- Staudacher, T., Allègre, C.J., 1988. Recycling of oceanic-crust and sediments — the noble gas subduction barrier. *Earth and Planetary Science Letters* 89, 173–183.
- Staudacher, T., Sarda, P., Richardson, S.H., Allègre, C.J., Sagna, I., Dmitriev, L.V., 1989. Noble-gases in basalt glasses from a mid-atlantic ridge topographic high at 14-degrees-N — geodynamic consequences. *Earth and Planetary Science Letters* 96, 119–133.
- Trieloff, M., Kunz, J., 2005. Isotope systematics of noble gases in the Earth's mantle: possible sources of primordial isotopes and implications for mantle structure. *Physics of the Earth and Planetary Interiors* 148, 13–38.
- Trieloff, M., Kunz, J., Clague, D.A., Harrison, D., Allègre, C.J., 2000. The nature of pristine noble gases in mantle plumes. *Science* 288, 1036–1038.
- Trieloff, M., Kunz, J., Allègre, C.J., 2002. Noble gas systematics of the Reunion mantle plume source and the origin of primordial noble gases in Earth's mantle. *Earth and Planetary Science Letters* 200, 297–313.
- Trieloff, M., Falter, M., Jessberger, E.K., 2003. The distribution of mantle and atmospheric argon in oceanic basalt glasses. *Geochimica Et Cosmochimica Acta* 67, 1229–1245.
- Yokochi, R., Marty, B., 2004. A determination of the neon isotopic composition of the deep mantle. *Earth and Planetary Science Letters* 225, 77–88.